OXFORD

Cerebral Cortex, 2023, **33**, 1074–1089
https://doi.org/10.1093/cercor/bhac121
Advance access publication date 30 March 2022
Original Article

Microanatomical study of pyramidal neurons in the contralesional somatosensory cortex after experimental ischemic stroke

Paula Merino-Serrais[1,2,*], Sergio Plaza-Alonso[1,2], Farida Hellal[3,4], Susana Valero-Freitag[3], Asta Kastanauskaite[1,2], Alberto Muñoz[1,2,5], Nikolaus Plesnila[3,6], Javier DeFelipe[1,2,7]

[1]Laboratorio Cajal de Circuitos Corticales, Centro de Tecnología Biomédica, Universidad Politécnica de Madrid, Madrid 28223, Spain,
[2]Departamento de Neurobiología Funcional y de Sistemas, Instituto Cajal, CSIC, Madrid 28002, Spain,
[3]Institute for Stroke and Dementia Research (ISD), University of Munich, Munich 81337, Germany,
[4]iTERM, Helmholtz center, Munich 85764, Germany,
[5]Departamento de Biología Celular, Universidad Complutense, Madrid 28040, Spain,
[6]Munich Cluster of Systems Neurology (Synergy), Munich 85764, Germany,
[7]Centro de Investigación Biomédica en Red sobre Enfermedades Neurodegenerativas. (CIBERNED), ISCIII, Madrid 28031, Spain

*Corresponding author: Laboratorio Cajal de Circuitos Corticales, Centro de Tecnología Biomédica, Universidad Politécnica de Madrid, Campus Montegancedo S/N, Pozuelo de Alarcón, Madrid 28223/Instituto Cajal (CSIC), Avenida Doctor Arce, 37, Madrid 28002, Spain. Email: paula.merino-serrais@cajal.csic.es

At present, many studies support the notion that after stroke, remote regions connected to the infarcted area are also affected and may contribute to functional outcome. In the present study, we have analyzed possible microanatomical alterations in pyramidal neurons from the contralesional hemisphere after induced stroke. We performed intracellular injections of Lucifer yellow in pyramidal neurons from layer III in the somatosensory cortex of the contralesional hemisphere in an ischemic stroke mouse model. A detailed 3-dimensional analysis of the neuronal complexity and morphological alterations of dendritic spines was then performed. Our results demonstrate that pyramidal neurons from layer III in the somatosensory cortex of the contralesional hemisphere show selective changes in their dendritic arbors, namely, less dendritic complexity of the apical dendritic arbor—but no changes in the basal dendritic arbor. In addition, we found differences in spine morphology in both apical and basal dendrites comparing the contralesional hemisphere with the lesional hemisphere. Our results show that pyramidal neurons of remote areas connected to the infarct zone exhibit a series of selective changes in neuronal complexity and morphological distribution of dendritic spines, supporting the hypothesis that remote regions connected to the peri-infarcted area are also affected after stroke.

Key words: cerebral cortex; dendritic spines; intracellular injections; neuronal complexity; tMCAo.

Introduction

Stroke is one of the major causes of death and disability worldwide (Donnan et al. 2008). While progress has been made in the prevention, treatment, and knowledge of stroke over the past decade, more effective therapeutic approaches are still needed to improve the quality of life of the patients. In this regard, a number of studies indicate that, after a stroke, remote regions connected to the infarcted area are also affected and may contribute to functional outcome. This process, known as diaschisis, occurs for example in the contralesional hemisphere, affecting the performance of the whole brain, and it may be involved in the suppression of functional recovery after stroke. Diaschisis can appear soon after ischemia and persist for weeks (Duering et al. 2012; Silasi and Murphy 2014; Buetefisch 2015). Currently, the primary mechanism of diaschisis is thought to be a loss of neuronal input from the damaged area, also defined as deafferentation (Butz et al. 2014). In humans, the neocortex is highly exposed to ischemic stroke, and in animal models of ischemia, it has been demonstrated that pyramidal neurons are more sensitive to ischemic stroke than other types of neuronal cells (Freund et al. 1990).

Pyramidal neurons are the most common cell type and the main projection neurons in the cerebral cortex. The dendritic structure of pyramidal neurons can be divided into 2 types according to their dendritic arbors—apical and basal. The apical dendritic arbor consists of a prominent main apical dendrite (arising from the upper pole of the pyramidal cell body) directed radially towards the pia mater, giving off several oblique apical collateral dendrites. In general, the distal portion of the apical dendrite forms a tuft of branches (apical dendritic tuft). The basal dendritic arbor is made out of a system of dendrites that arise from 3 to 6 primary dendrites from the base of the soma, which are directed laterally or downwards (DeFelipe and Fariñas 1992).

Received: August 6, 2021. **Revised:** March 1, 2022. **Accepted:** March 2, 2022

In addition, it is well established that the basal and apical arbors have different morphological and functional features and are involved in different synaptic circuits (DeFelipe and Fariñas 1992; Spruston 2008; Larkum 2013; Harris and Shepherd 2015; Mel et al. 2017; Gidon et al. 2020). More specifically, in the somatosensory cortex (SSCx), it has been shown that the precise function of the pyramidal neurons depends on the cortical layer location (see for example Brecht 2017).

The pattern of dendritic arborization of a pyramidal neuron is related to the degree of information integration and synaptic plasticity induction. It is widely accepted that the dendritic tree structure influences the biophysical and computational properties of neurons, modulating the cortical circuitry (Häusser et al. 2000; DeFelipe 2011; Stuart and Spruston 2015). The shape of the dendritic arbors of pyramidal neurons has been linked to a maximization of the connectivity patterns between dendrites and surrounding axons (Wen et al. 2009; Tang et al. 2019). It has been suggested that dendritic arbors are the synaptic input units rather than individual dendrites, in line with the notion that dendritic spines are part of a complex system as opposed to being single functional units (Jia et al. 2010; Leguey et al. 2018). Furthermore, dendritic spines (for simplicity, spines) are considered as the major postsynaptic elements of excitatory glutamatergic synapses (DeFelipe and Fariñas 1992; Harris and Kater 1994; DeFelipe 2015). Therefore, changes in the number of spines are indicative of differences in the number of excitatory inputs that pyramidal cells receive. Moreover, spines are plastic structures and are considered crucial to memory, learning, and cognition—and their formation and elimination have been linked to memory storage capacity (Bourne and Harris 2007; Spruston 2008; Yuste 2010; Kandel et al. 2014; DeFelipe 2015).

Therefore, analyzing possible microanatomical changes in pyramidal neurons under different pathological conditions—such as after an ischemic stroke—provides an excellent opportunity to study neuronal dysfunction in cortical circuits, offering useful information to develop new diagnostic approaches and treatments for patients with focal or global cerebral ischemia.

In this regard, synaptic failure has been described as a key process in neuronal damage in ischemic stroke, even in the absence of neuronal death (Jeannette and van Putten 2012). In the ipsilateral hemisphere, alterations in neuronal complexity and synaptic plasticity have been suggested as valuable therapeutic targets (Takamatsu et al. 2016; Zhu et al. 2017; Lin et al. 2018; Xie et al. 2019).

However, pyramidal neurons in distinct cortical regions and in different layers participate in different synaptic circuits and cortical functions (Barbas 2015; D'Souza and Burkhalter 2017; Rockland 2019). Furthermore, there are significant differences in the microanatomy of these cells between cortical areas in the mouse cerebral cortex (Benavides-Piccione et al. 2006; Ballesteros-Yáñez et al. 2010). Moreover, it has been reported that the SSCx is especially vulnerable to ischemic insults, with pyramidal neurons from layer III being exceptionally sensitive to ischemia (Lin et al. 1990). In this regard, pyramidal neurons from layer III have been suggested as the main transcallosal projection neurons in the cerebral cortex (Chovsepian et al. 2017). The SSCx has been described as a crucial region in the processing of afferent somatosensory inputs and is essential for emotion processing, including the generation of emotional states and sensorimotor integration. SSCx function is involved in each stage of emotion processing and therefore plays an important role in the pathophysiology of many neuronal disorders (Kropf et al. 2018).

In the present study, we have analyzed whether neuronal complexity, spine density, and morphology are impaired in the contralesional hemisphere after induced stroke using intracellular injections. Since this technique—together with the reconstruction of the labeled cells—represents a very time-consuming approach, we chose to study the structure of layer III pyramidal neurons, which probably project to the ischemic lesions (Fenlon et al. 2017). For this purpose, we performed intracellular injections of Lucifer yellow (LY) in pyramidal neurons from layer III in the SSCx of the contralesional hemisphere in an ischemic mouse model that produces a large ipsilateral lesion. Our results show that in the contralesional SSCx, pyramidal neurons from layer III show certain morphological alterations, mostly leading to less complexity of the apical dendritic arbor, including a significant decrease in dendritic length and dendritic volume. In addition, we found differences in spine morphology in both apical (main apical and collateral dendrites) and basal dendrites, but no changes in their density. Thus, the present results show a series of selective changes in pyramidal neurons in the contralesional SSCx after a large lesion induced by an experimental stroke.

Materials and methods

tMCAo model

Experiments were performed on adult male C57BL/6N mice (12–16 weeks old; body weight, 23–26 g; Charles Rivers Laboratories). All experimental procedures were conducted in accordance with European regulations, the ethical committee of Upper Bavaria (Vet 2-15-196) and in compliance with the ARRIVE (Animal Research: Reporting In Vivo Experiments) criteria (Kilkenny et al. 2010).

The left middle cerebral artery (MCA) was occluded for 60 min, inducing a transient cerebral ischemia (tMCAo). The mice were anesthetized with 4% isoflurane (balanced with 30% O_2 and 65% N_2) and maintained with 1.5%–2% isoflurane for the duration of surgery. The body temperature was maintained at 37 °C using a feedback-controlled heating pad. A silicon-coated filament (# 701912PK5Re, Doccol) was inserted and pushed through the common carotid artery until the MCA had been

reached. Reperfusion was induced by withdrawal of the filament after 1 h of occlusion, as previously described elsewhere (Lourbopoulos et al. 2017). The occlusion was confirmed by decreased regional cerebral blood flow monitored by a laser Doppler probe fixed to the skull above the tMCAo territory and the vital parameters were monitored by a pulse oximeter (Supplementary Fig. 1). Wounds were treated with povidone-iodine and sutured; the mice received an injection of saline (1 mL s.c.; B Braun Melsungen) and were placed in a 32 °C recovery chamber until motor function had been fully recovered. The mice were then returned to their home cage and received postoperative care, including injections of fluids and jelly food feeding supplemented at the bottom of the cage for 10 days, as previously described elsewhere (Lourbopoulos et al. 2017). Sham-operated mice underwent the same surgery without occlusion of the MCA and followed the same postoperative care.

Intracellular injections and confocal microscopy

For intracellular injections, 12 weeks after tMCAo induction, the animals were anesthetized by intraperitoneal injection of midazolam (5 mg/kg; Braun, Melsungen, Germany), fentanyl (0.05 mg/kg; Jansen-Cilag, Neuss, Germany), and medetomidine (0.5 mg/kg; Pfizer, Karlsruhe, Germany)—and then intracardially perfused with phosphate buffer pH 7.4 (PB) followed by 4% paraformaldehyde (PFA). The brains were then postfixed in PFA for 24 h.

Coronal sections (150 μm thick) were obtained on a vibratome and were then prelabeled with 4,6-diamino-2-phenylindole (DAPI; Sigma, St. Louis, MO) to visualize the nuclei. Pyramidal neurons from layer III in the Barrel field of the SSCx were individually injected with LY by continuous current, as previously described (Benavides-Piccione et al. 2013). Finally, the sections were mounted in glycerol (50% in 0.1 M PB, 0.1% azide) and studied via confocal microscopy. The sections immediately adjacent (50 μm either side of the 150 μm thick sections) were Nissl-stained in order to identify the cortical areas and the extent of the ischemic lesson.

This intracellular injection technique exhibits several methodological limitations, reducing the total number of LY-injected neurons that are suitable for the statistical analysis. Unfortunately, the diffusion of the LY up to the tip of the dendrites fails in many neurons and, therefore, they have to be discarded from the analysis. In addition, the percentage of the basal and apical arbors included may vary depending on how parallel the main apical dendrite runs with respect to the surface of the slice and how deep in the section the labeled neuron is located. In the present study, the statistical analysis of the main apical dendrites included only neurons that showed a main apical dendrite with a length of at least 180 μm (see Benavides-Piccione et al. 2020 for further details).

Imaging was performed with a ZEN inverted scanning confocal system (Zeiss LSM 710; Carl Zeiss Microscopy GmbH, Jena, Germany) using a 488 nm Argon laser and 405 nm UV. The fluorescence of DAPI and Alexa 488 was recorded through separate channels.

For spine morphology analyses, complete dendrites were recorded in image stacks at 0.14 μm intervals with a 63× oil immersion lens (Numerical aperture, NA: 1.40; refraction index, 1.45) and zoom 2.3 (image resolution: 1,024 × 1,024 pixels; pixel size: 0.06 μm). No pixels were saturated within the dendritic spines.

For neuronal reconstruction, neurons from layer III of the SSCx were recorded at 0.45 μm intervals with a 40× oil immersion lens (NA: 1.3; refraction index, 1.51) and 0.9 zoom (image resolution: 1,024 × 1,024 pixels; pixel size: 0.23 μm). After acquisition, the stacks were coded to randomize the stroke and sham conditions and these codes were not broken until the quantitative analysis had been completed.

3D reconstruction

Neurons were reconstructed in 3D using Neurolucida 360 software (MicroBrightField Inc., Williston, VT). The confocal images of the dendritic arbors were analyzed by tracing the neuronal structure in both apical and basal dendritic trees. After tracing, the reconstructed data were exported to Neurolucida Explorer (MicroBrightField Inc., Williston, VT) for quantitative analysis.

Dendritic arbor complexity was assessed by measuring several morphological parameters as a function of the distance from the soma, creating concentric spheres—centered on the cell body—of increasing 10 μm radii (Sholl analysis). All the morphological parameters analyzed in the present study (dendritic length, dendritic volume, number of intersections, number of nodes, dendritic surface area, and dendritic diameter) were calculated using Neurolucida Explorer as described in Benavides-Piccione et al. (2006).

Regarding spine density and spine morphology analyses, for main apical dendrites, only 100 μm of dendritic length from the cell body were included in the analysis. In apical collateral and basal dendrite analyses, only complete dendrites were analyzed. In addition, spine density in main apical, apical collateral, and basal dendrites was calculated for each dendrite by dividing the number of spines by dendritic length. For spine analysis, the spines were marked during tracing with all protrusions considered as spines, applying no correction factors to the spine counts. For further analysis, spine density, spine volume, and spine length per dendrite were measured as a function of the distance from the soma for main apical and basal dendrites and from the apical trunk for apical collateral dendrites.

Immunofluorescence and synaptopodin-positive puncta quantification analysis

Free-floating coronal sections (50 μm thick) were used for double immunofluorescence. First, the slices were blocked for 1 h in PB (0.1 M) with 0.25% Triton X-100 and 3% normal goat serum (Vector Laboratories Inc., Burlingame, CA, USA). The sections were then incubated

at 4 °C for 48–72 h in the same solution with rabbit anti-synaptopodin (SE-19; S9442; Sigma; 1:500) and mouse anti-NeuN (1:2,000, Chemicon) primary antibodies. After rinsing in PB, the sections were incubated for 2 h at room temperature with Alexa Fluor 488-coupled goat anti-rabbit and Alexa Fluor 594-coupled goat anti-mouse antibodies (1:1,000; Molecular Probes). The sections were then rinsed in PB, counterstained with DAPI, mounted, and coverslipped with ProLong Gold antifade reagent for immunofluorescence analysis (Life Technologies, Carlsbad, CA).

For synaptopodin-positive puncta quantification analysis, confocal microscopy was performed with a Zeiss LSM 710. Synaptopodin and NeuN immunostaining and DAPI staining were recorded through separate channels with a 63× objective (NA, 1.4). Z depth in every confocal stack was 0.14 μm. We scanned 10 image stacks from layer II to III of the SI (barrel field) and SII regions contralesional to surgery in tMCAo and sham-operated animals. For the quantification of the synaptopodin-positive puncta, Image J software (a 3D object counting tool) was used. The image stacks were cropped to ensure that they were restricted to areas of neuropil. Synaptopodin fluorescence was automatically enhanced, and then single-pixel background fluorescence was eliminated by despeckling. The 3D object counting tool was then applied to collect data regarding the number of synaptopodin-immunoreactive (Sypo-ir) punctate elements, excluding those in contact with exclusion borders. Density values were obtained after normalization of the number of synaptopodin-positive puncta to the tissue volume of each stack.

Statistical analysis

To assure impartiality, all morphological analyses were performed blindly. The animals were coded and the assigned code was kept until the analyses were completed. To test the overall effect, unpaired Mann–Whitney test was used to compare the averages. To compare values as a function of the distance from the soma, Two-way ANOVA repeated measures (P and F values + interaction; degrees of freedom, df) followed by a post hoc multiple Bonferroni test were used. Kolmogorov–Smirnov test was used to perform the frequency distribution analyses. Data values are expressed as mean ± SEM. In all cases, $P < 0.05$ was considered to be significant (* < 0.05, ** < 0.01).

Results

To examine whether ischemic stroke could induce microanatomical alterations in the contralesional hemisphere, we performed 594 intracellular injections with LY in pyramidal neurons from layer III in the SSCx of 5 sham-operated and 5 tMCAo mice (Fig. 1 and Supplementary Fig. 2).

Stroke decreases neuronal complexity in apical dendritic arbors of the contralesional hemisphere

To study if neuronal structure in the contralesional hemisphere could be altered after stroke, we evaluated the neuronal complexity of the dendritic arborization in both apical and basal dendritic arbors by measuring dendritic length, dendritic volume, number of intersections, number of nodes, dendritic surface area, and dendritic diameter (Fig. 2). All the morphometric parameters were analyzed as a function of the distance from the soma (Sholl analysis). In sections from tMCAo mice, only LY-injected neurons in the contralesional SSCx were selected for the analysis. For statistical analysis in apical arbors, 30 individual branches per group were analyzed. We found that the dendrites were significantly shorter in tMCAo compared to sham-operated mice (sham-operated = 73.82 ± 12.77 μm, tMCAo = 55.42 ± 9.4 μm; Sholl analysis = Two-way ANOVA, $P < 0.0001$; $F = 4.96$, df12; Bonferroni post hoc test $P < 0.05$; Fig. 3A). Dendritic volume was also significantly lower in tMCAo mice compared to sham-operated (sham-operated = 53.87 ± 6.77 μm^3, tMCAo = 44.17 ± 5.89 μm^3; Sholl analysis = Two-way ANOVA, $P = 0.0008$; $F = 2.85$, df12; Bonferroni post hoc test $P < 0.05$; Fig. 3B). Similar significantly lower values were found for the number of intersections (sham-operated = 5.54 ± 0.89, tMCAo = 4.21 ± 0.66; Sholl analysis = Two-way ANOVA, $P < 0.0001$; $F = 4.31$, df12; Bonferroni post hoc test $P < 0.05$; Fig. 3C) and dendritic surface area (sham-operated = 208.4 ± 31.88 μm^2, tMCAo = 162.6 ± 24.55 μm^2; Sholl analysis = Two-way ANOVA, $P < 0.0001$; $F = 4.56$, df12; Bonferroni post hoc test $P < 0.05$; Fig. 3D). However, no significant differences were found in tMCAo mice regarding the number of nodes (sham-operated = 1.07 ± 0.21, tMCAo = 0.78 ± 0.18; Sholl analysis = Two-way ANOVA, $P = 0.2$; $F = 1.32$, df12; Fig. 3E) and dendritic diameter (sham-operated = 0.99 ± 0.13 μm, tMCAo = 1.04 ± 0.13 μm; Sholl analysis = Two-way ANOVA, $P = 0.99$; $F = 0.21$, 12df; Fig. 3F). All statistical data are provided in Supplementary Tables 1 and 2.

Basal dendritic arbor complexity remains unaltered after ischemic stroke in the contralesional hemisphere

For the analysis of the neuronal complexity in basal arbors, we analyzed 30 individual branches per group. In basal dendritic arbors, none of the parameters analyzed yielded statistically significant differences between the 2 groups: dendritic length (sham-operated = 141 ± 21.7 μm, tMCAo = 147.6 ± 23.23 μm; Sholl analysis = Two-way ANOVA, $P = 0.94$; $F = 0.16$, df11; Fig. 4A), dendritic volume (sham-operated = 88.11 ± 10.60 μm^3, tMCAo = 84.25 ± 10.49 μm^3; Sholl analysis = Two-way ANOVA, $P = 0.70$; $F = 0.29$, df11; Fig. 4B), number of intersections (sham-operated = 12.39 ± 1.71, tMCAo = 11.89 ± 1.72; Sholl analysis = Two-way ANOVA, $P = 0.98$; $F = 0.15$, df11; Fig. 4C), dendritic surface area (sham-operated = 376.3 ± 51.62 μm^2, tMCAo = 368.2 ± 52.32 μm^2; Sholl analysis = Two-way ANOVA, $P = 0.90$; $F = 0.22$, df11; Fig. 4D), number of

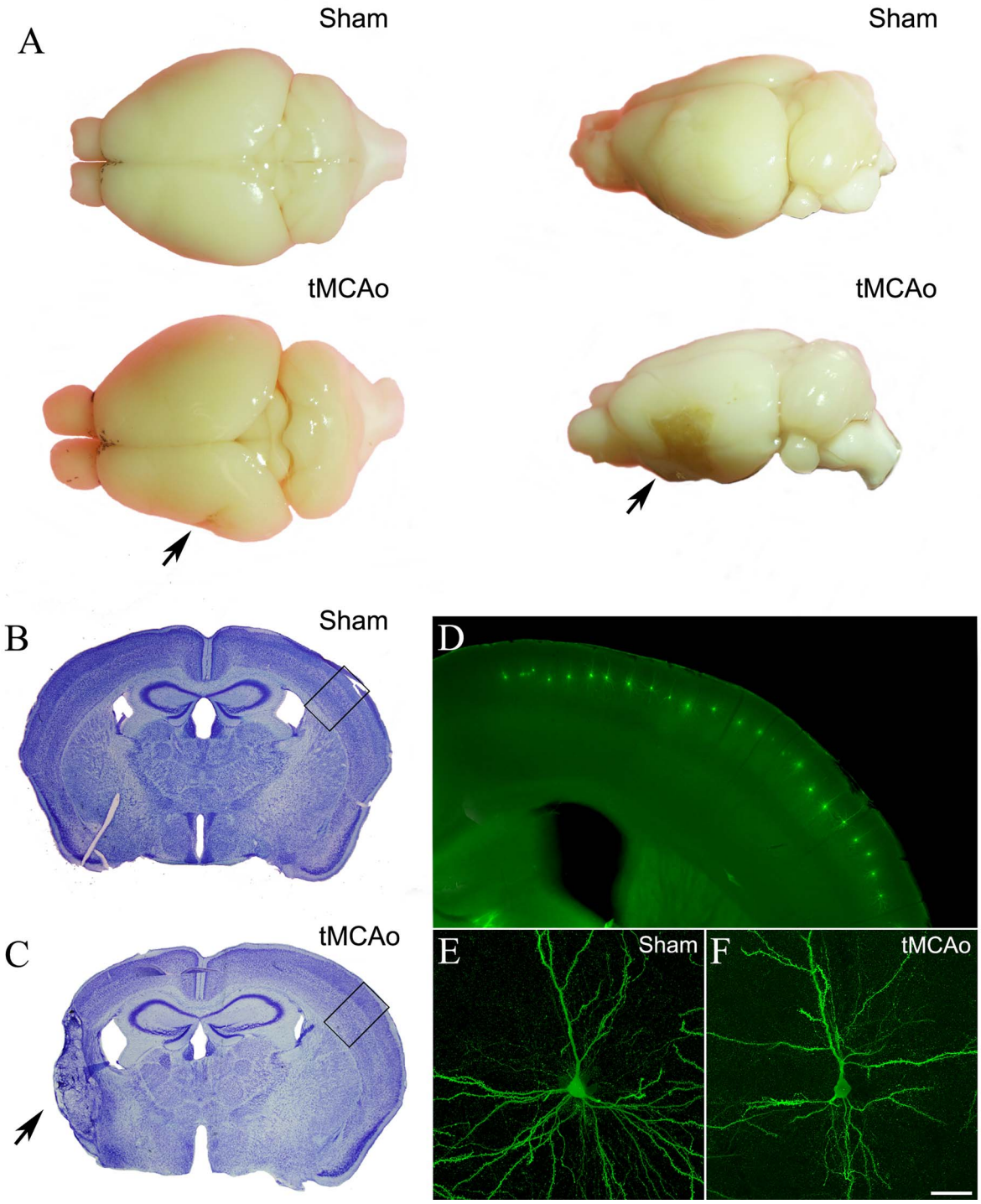

Fig. 1. Characterization of the ischemic lesion extent and LY-intracellular injections in the SSCx. A) Macroscopic images of sham-operated and tMCAo mice showing the ischemic lesion in the left hemisphere (arrow). B, C) Coronal sections stained with Nissl in sham-operated (B) and tMCAo (C) mice. Black boxes indicate the area of interest. D–F) Images showing the LY-intracellular injections performed in pyramidal neurons in the SSCx. D) Panoramic view in sham-operated mouse and (E, F) higher magnification confocal pictures showing pyramidal neurons individually injected in sham-operated (E) and tMCAo (F) mice. Scale bar in F indicates 2 mm in A, 1 mm in B–C, 500 μm in D, and 30 μm in E–F.

nodes (sham-operated = 1.66 ± 0.48, tMCAo = 1.66 ± 0.50; Sholl analysis = Two-way ANOVA, $P = 0.84$; $F = 0.53$, df11; Fig. 4E), or dendritic diameter (sham-operated = 0.86 ± 0.11 μm, tMCAo = 0.87 ± 0.11 μm; Sholl analysis = Two-way ANOVA, $P = 0.99$; $F = 0.05$, df11; Fig. 4F). All statistical data are provided in Supplementary Table 3.

Dendritic spine density is unaltered in the contralesional hemisphere after stroke

A detailed analysis of the spine density was performed in apical (main apical and collateral dendrites) and basal dendrites from SSCx pyramidal neurons in the contralesional hemisphere (Fig. 5). No statistical differences were

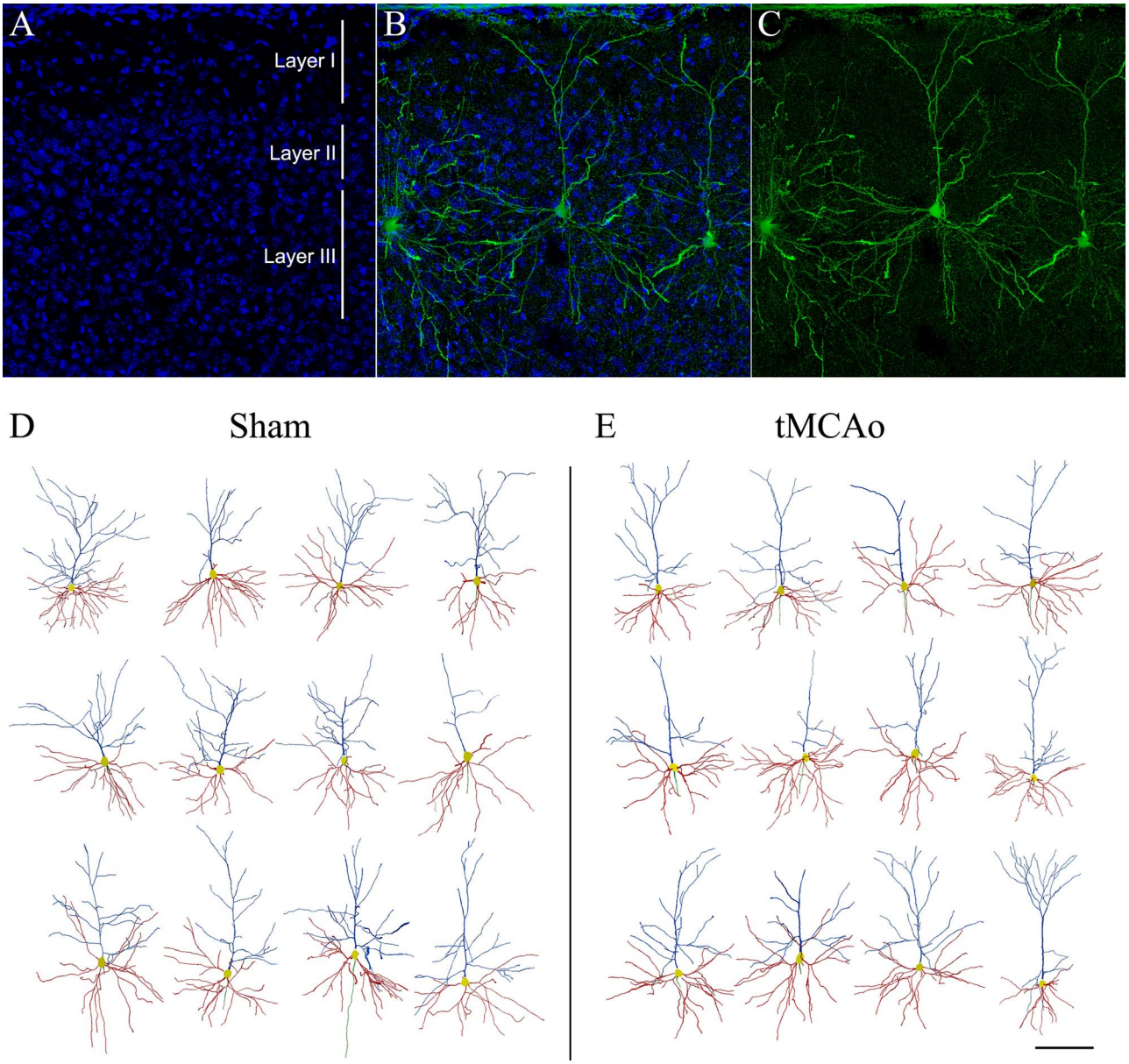

Fig. 2. LY-injected and reconstructed pyramidal neurons in SSCx. A–C) Confocal microscopy pictures of an individual LY-injected neuron in layer III of the SSCx showing (A) DAPI staining (in blue), (C) the LY-injected neuron (in green), and (B) the merge of A and C. D, E) Drawings of the apical dendritic arbors (blue), basal dendritic arbors (red), and initial portion of the axons (green) of pyramidal neurons from layer III of the SSCx in sham-operated (D) and tMCAo (E) mice (Neurolucida Explorer). Scale bar shown in E indicates 120 μm in A–C and 150 μm in D–E.

found between the sham-operated and tMCAo groups with regard to main apical, apical collateral, or basal dendrites (Fig. 6).

For the main apical dendrite analysis, spine density was measured assessing a total dendritic length of 2,100 μm in sham-operated mice (21 dendrites; 0.69 ± 0.04 spines/μm, 1,795 spines) and 1,900 μm in tMCAo mice (20 dendrites; tMCAo: 0.79 ± 0.04 spines/μm, 1,966 spines; Mann–Whitney, $P = 0.12$; Fig. 6A).

In the apical collateral dendrite analysis, 21 dendrites per group were included. Spine density was measured assessing a total dendritic length of 2,390 μm in sham-operated and 2,130 μm in tMCAo mice (sham-operated 1.12 ± 0.06 spines/μm, 3,088 spines; tMCAo: 1.22 ± 0.05 spines/μm, 2,945 spines; Mann–Whitney test, $P = 0.21$; Fig. 6C). In the case of the basal dendrite analysis, 31 dendrites per group were included. Spine density was measured assessing a total dendritic length of 3,640 μm in sham-operated and 3,830 μm in tMCAo mice (sham-operated 1.18 ± 0.05 spines/μm, 4,343 spines; tMCAo: 1.19 ± 0.03 spines/μm, 4,254 spines; Mann–Whitney, $P = 0.65$; Fig. 6E).

As seen in Fig. 6, no significant differences in dendritic spine density as a function of the distance from the soma were found between the sham-operated and tMCAo groups for either main apical, apical collateral, or basal dendrites (Two-way ANOVA, $P > 0.05$; $F = 1.51$, df10; $F = 1.45$, df6; and $F = 1.75$, df7; Fig. 6B, D, and F, respectively).

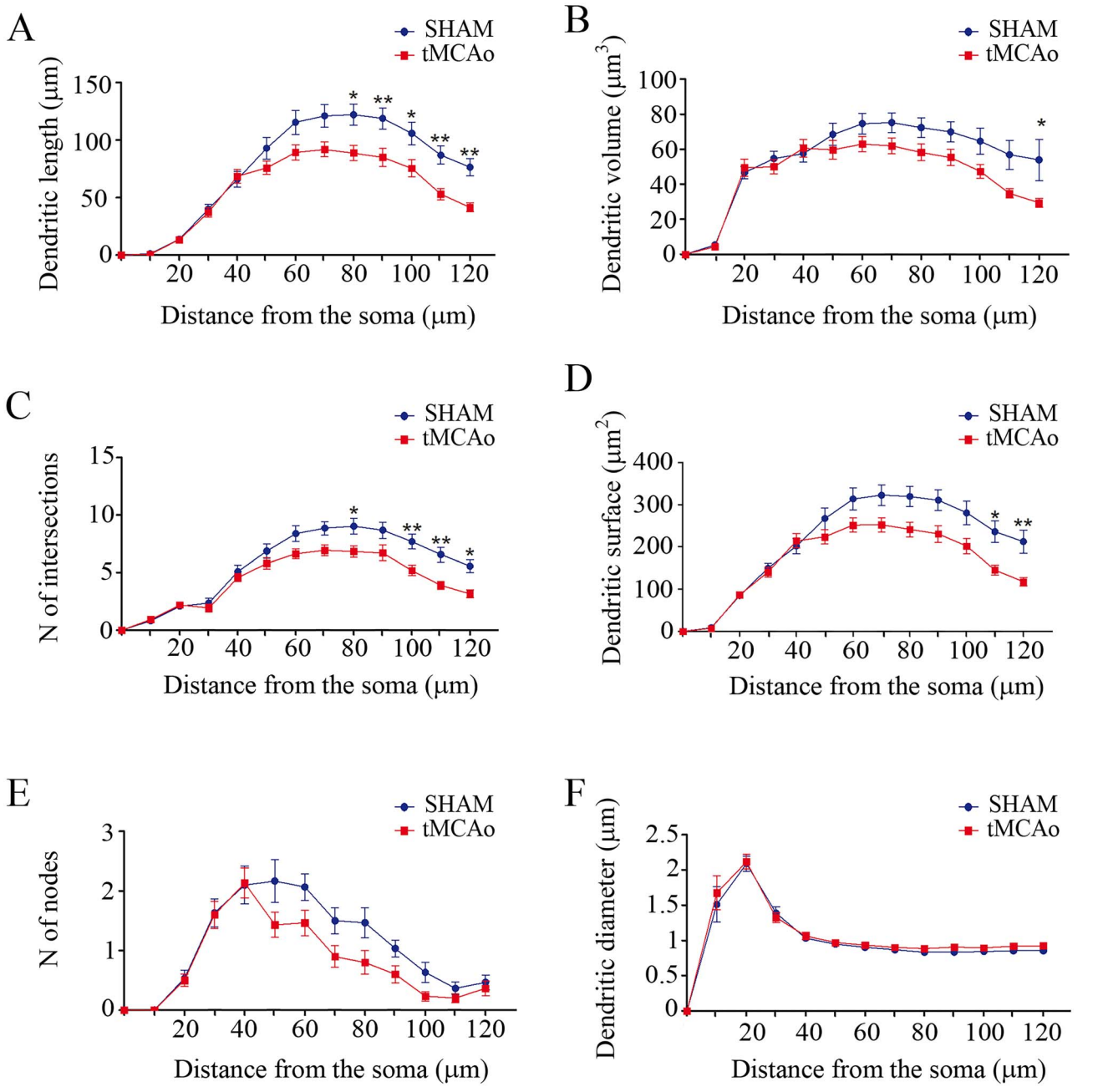

Fig. 3. Apical dendritic arbors show lower neuronal complexity in tMCAo mice. Comparative morphometric analysis of A) dendritic length, B) dendritic volume, C) number of intersections, D) dendritic surface area, E) number of nodes, and F) dendritic diameter, as a function of the distance from the soma (Two-way ANOVA repeated measures followed by a post hoc multiple Bonferroni test). *$P < 0.05$, **$P < 0.01$.

Stroke induces dendritic spine morphology differences in both apical and basal dendrites

Analyses of dendritic spine morphology were performed in apical (main apical and collateral dendrites) and basal dendrites.

In the main apical dendrite analysis, no significant differences were found in spine volume between groups when it was analyzed as an average (sham-operated: 0.1 ± 0.04 μm^3; tMCAo: 0.1 ± 0.03 μm^3; Mann–Whitney test; $P = 0.7$; Fig. 7A); likewise, no significant differences were found when analyzed as a function of the distance from the soma (Two-way ANOVA, $P > 0.05$; $F = 1.69$, df8; Fig. 7B). Moreover, no difference was found in the spine length average between tMCAo (1.21 ± 0.04 μm) and sham-operated mice (1.31 ± 0.06 μm; Mann–Whitney test; $P = 0.3$; Fig. 7C)—or when analyzing spine length as a function of the distance from the soma (Two-way ANOVA, $P > 0.05$; $F = 1.13$, df8; Fig. 7D).

Regarding apical collateral dendrites, no significant differences were found in spine volume between groups when it was analyzed as an average (sham-operated: 0.16 ± 0.009 μm^3; tMCAo: 0.16 ± 0.008 μm^3; Mann–Whitney test; $P = 0.8$; Fig. 7E); likewise, no significant differences were found when analyzed as a function of the distance from the soma (Two-way ANOVA, $P = 0.04$; $F = 2.0$, df7; Fig. 7F). Moreover, no

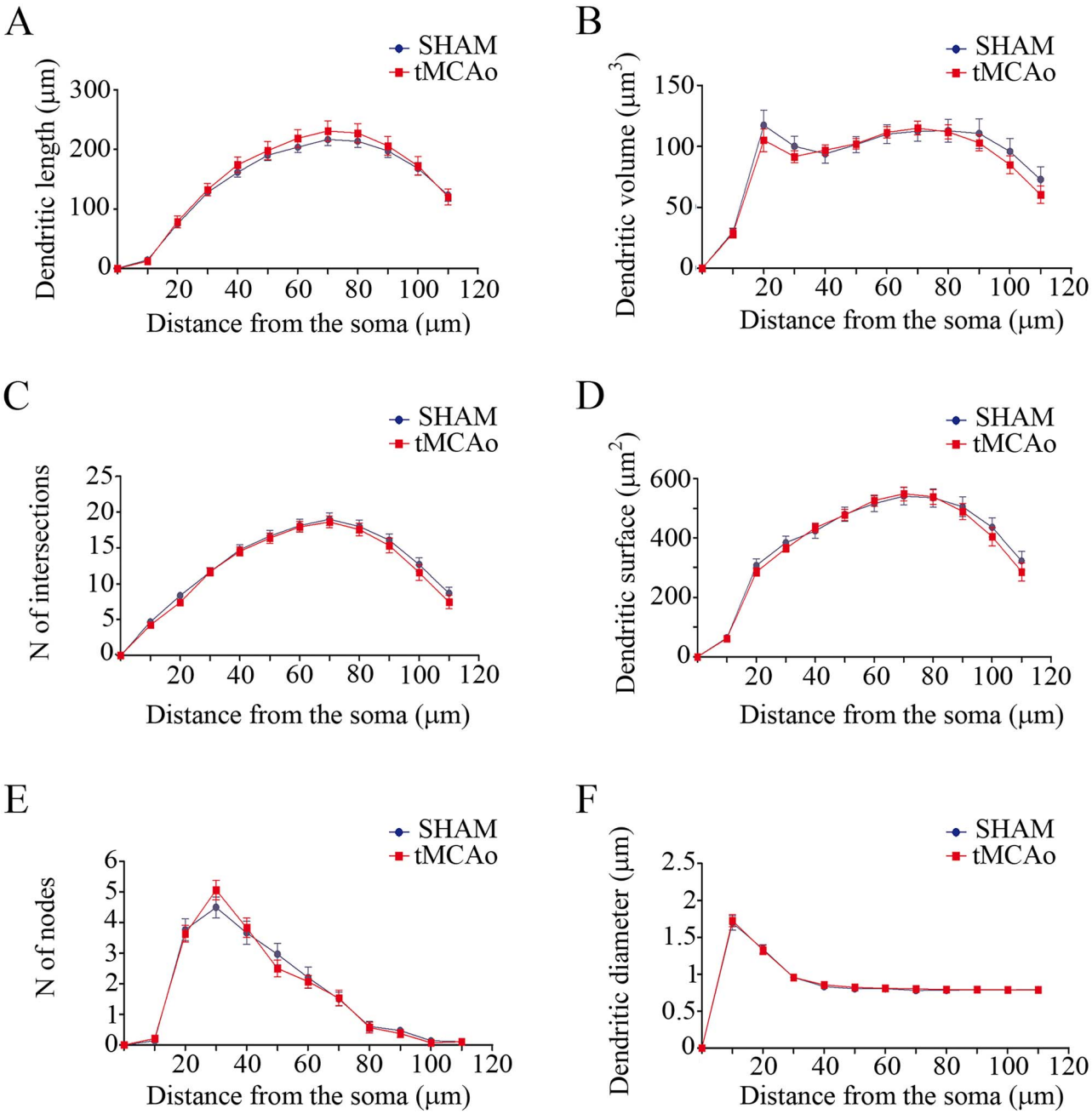

Fig. 4. Basal dendritic arbor complexity remains unaltered in tMCAo mice. Comparative morphometric analysis of A) dendritic length, B) dendritic volume, C) number of intersections, D) dendritic surface area, E) number of nodes, and F) dendritic diameter, as a function of the distance from the soma (Two-way ANOVA repeated measures followed by a post hoc multiple Bonferroni test).

difference was found in the spine length average between tMCAo (1.41 ± 0.06 μm) and sham-operated mice (1.56 ± 0.05 μm; Mann–Whitney test; $P = 0.06$; Fig. 7G)—or when analyzing spine length as a function of the distance from the soma (Two-way ANOVA, $P > 0.05$; $F = 1.89$, df7; Fig. 7H).

Similarly, in the basal dendrite analysis, no significant differences were found in spine volume between groups when it was analyzed as an average (sham-operated 0.16 ± 0.009 μm^3; tMCAo: 0.18 ± 0.007 μm^3; Mann–Whitney test; $P = 0.07$; Fig. 7I) neither as a function of the distance from the soma (Two-way ANOVA, $P > 0.05$; $F = 1.22$, df8; Fig. 7J). Moreover, no difference was found in the spine length average between tMCAo (1.40 ± 0.02 μm) and sham-operated mice (1.45 ± 0.04 μm; Mann–Whitney test; $P = 0.45$; Fig. 7K)—or when analyzing spine length as a function of the distance from the soma (Two-way ANOVA, $P > 0.05$; $F = 0.68$, df8; Fig. 7L).

However, further analysis of the frequency distribution of the spine length and spine volume showed a significant difference depending on the type of dendrite between tMCAo mice and sham-operated mice. Using frequency distribution analysis, in main apical dendrites, statistical differences were found between groups

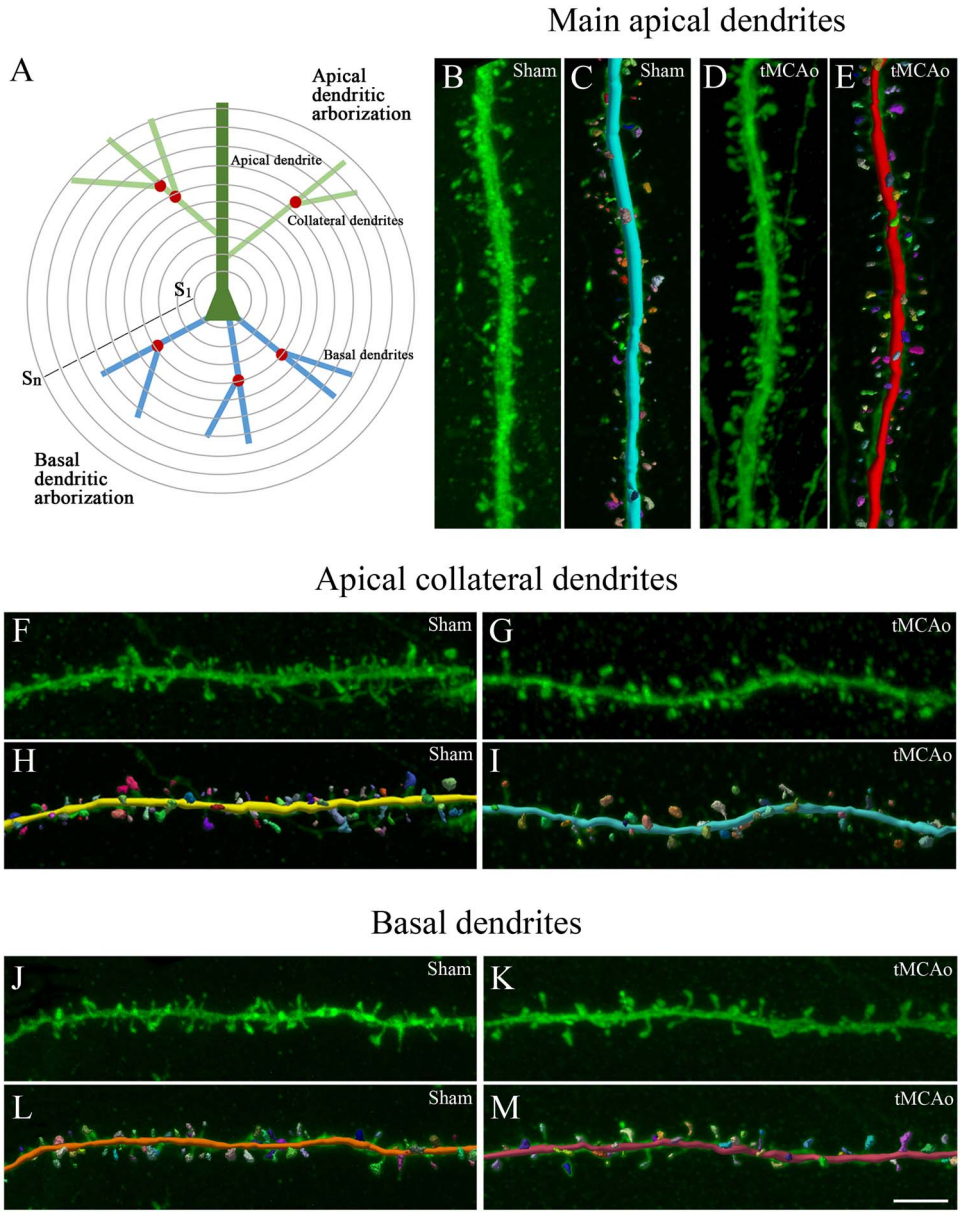

Fig. 5. 3D neuronal and spine reconstruction. A) Schematic drawing showing the pyramidal neuron structures that were analyzed using Sholl analysis ($S_1 \ldots S_n$; concentric spheres per distance from the soma): apical dendrite, collateral dendrites, basal dendrites. Nodes are indicated with a red circle and dendritic spines are not represented. B–M) 3D dendritic reconstruction for spine morphology analysis. B–E) Main apical, F–I) apical collateral, and J–M) dendritic segments from LY-injected pyramidal neurons in SSCx from (B, F, J) sham-operated and (D , G, K) tMCAo mice. C, E, H, I, L and M) The same dendritic segments as in B, D, F, G, J, and K, respectively, showing the 3D spine reconstruction process. Scale bar shown in M indicates 3 μm in B–M.

when we analyzed spine volume (Kolmogorov–Smirnov, $P = 0.004$; Fig. 8A); however, no differences were found regarding spine length (Kolmogorov–Smirnov, $P > 0.05$; Fig. 8B).

In addition, no differences in apical collateral dendrites were found between groups when we analyzed spine volume (Kolmogorov–Smirnov, $P > 0.05$; Fig. 8C). However, statistical differences were found regarding spine length (Kolmogorov–Smirnov, $P > 0.05$; Fig. 8D) when we compared tMCAo with sham-operated animals. In basal dendritic arbors, we found statistical differences between the 2 groups with regard to both spine volume and spine length (Kolmogorov–Smirnov, $P < 0.0001$ and $P = 0.0039$, respectively; Fig. 8E and F).

Lack of changes in the density of Sypo-ir puncta in the neuropil

The density of Sypo-ir puncta was analyzed in the neuropil of layers II–III from SI (barrel field) and SII neocortical regions of the contralesional hemisphere, in tMCAo and sham-operated mice (Supplementary Fig. 3). This analysis was performed in 10 confocal stacks per case and region, taken from Sypo-ir and NeuN double-immunostained sections, counterstained with DAPI. Avoidance of NeuN- and DAPI-stained elements allowed the identification of neuropil regions that were cropped, in 3D, from original confocal stacks in order to estimate in 3D the density of Sypo-ir puncta per unit volume (Supplementary Fig. 3C–F). In layer III

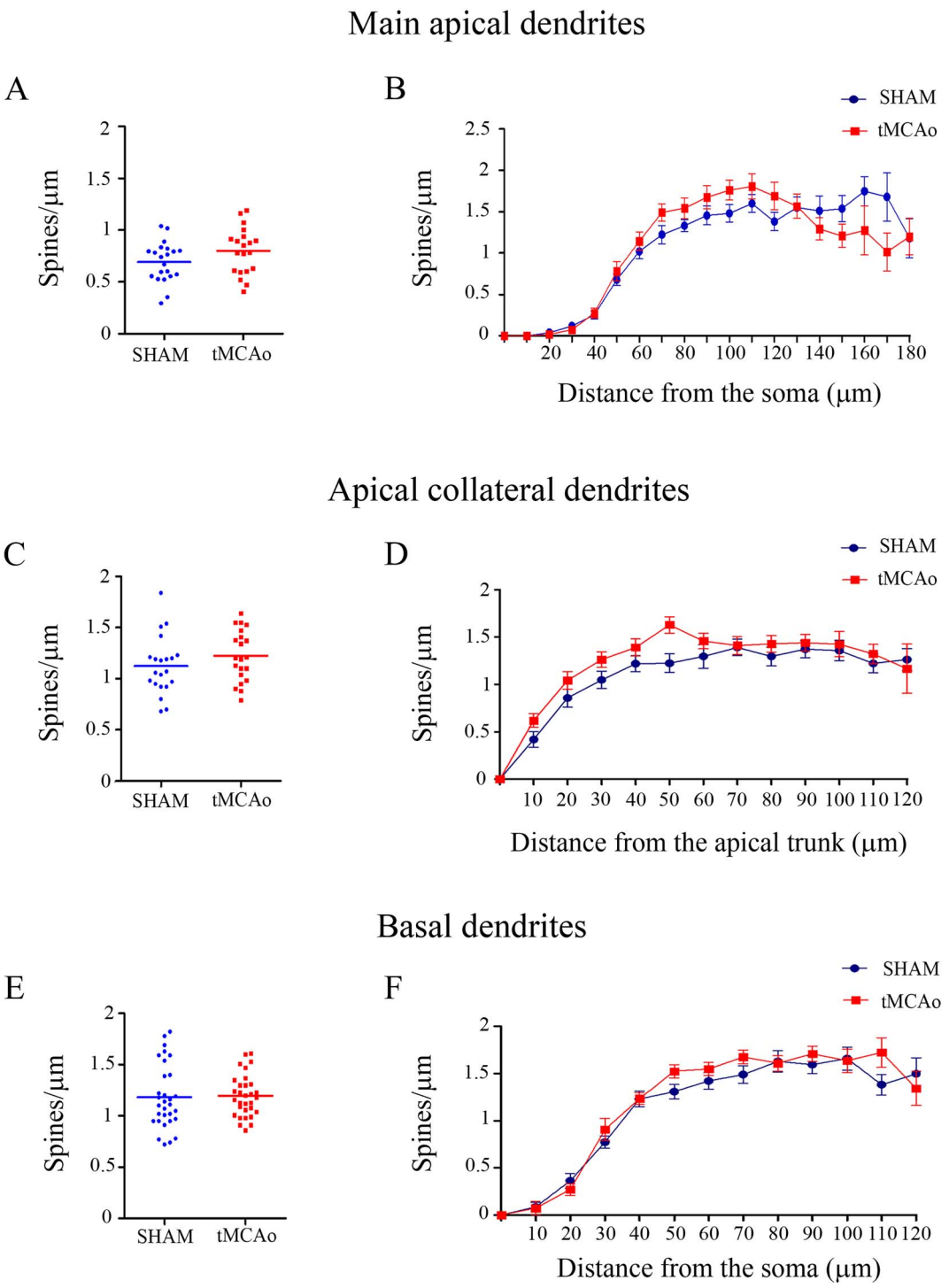

Fig. 6. Comparative morphometric analysis of the spine density in pyramidal neurons from the contralesional SSCx. Spine density analysis (spines/μm) showing (A, C, E) the average spine density per dendrite in main apical dendrites (A), apical collateral dendrites (C), and basal dendrites (E) (unpaired Mann–Whitney test)—and B, D, F) the spine density as a function of the distance from the soma (Two-way ANOVA repeated measures) in main apical dendrites (B), apical collateral dendrites (D), and basal dendrites (F).

neuropil of SII, the number of Sypo-ir puncta/μm^3 was very similar in tMCAo (207.0 ± 5.71) and sham-operated (209.7 ± 3.36) groups, and no significant differences were found between them (unpaired Mann–Whitney test). Similarly, in layer III neuropil of SI (barrel field), no statistically significant differences in Sypo-ir puncta density values were found between tMCAo (217.9 ± 5.96) and sham-operated animals (213.9 ± 3.21).

Discussion

Stroke is one of the leading causes of permanent adult disability and death in the aging population worldwide (Feigin et al. 2017). Although great advances have been made with regard to this medical condition, a better understanding of the underlying pathological process after stroke is needed. Nowadays, neuronal reorgani-

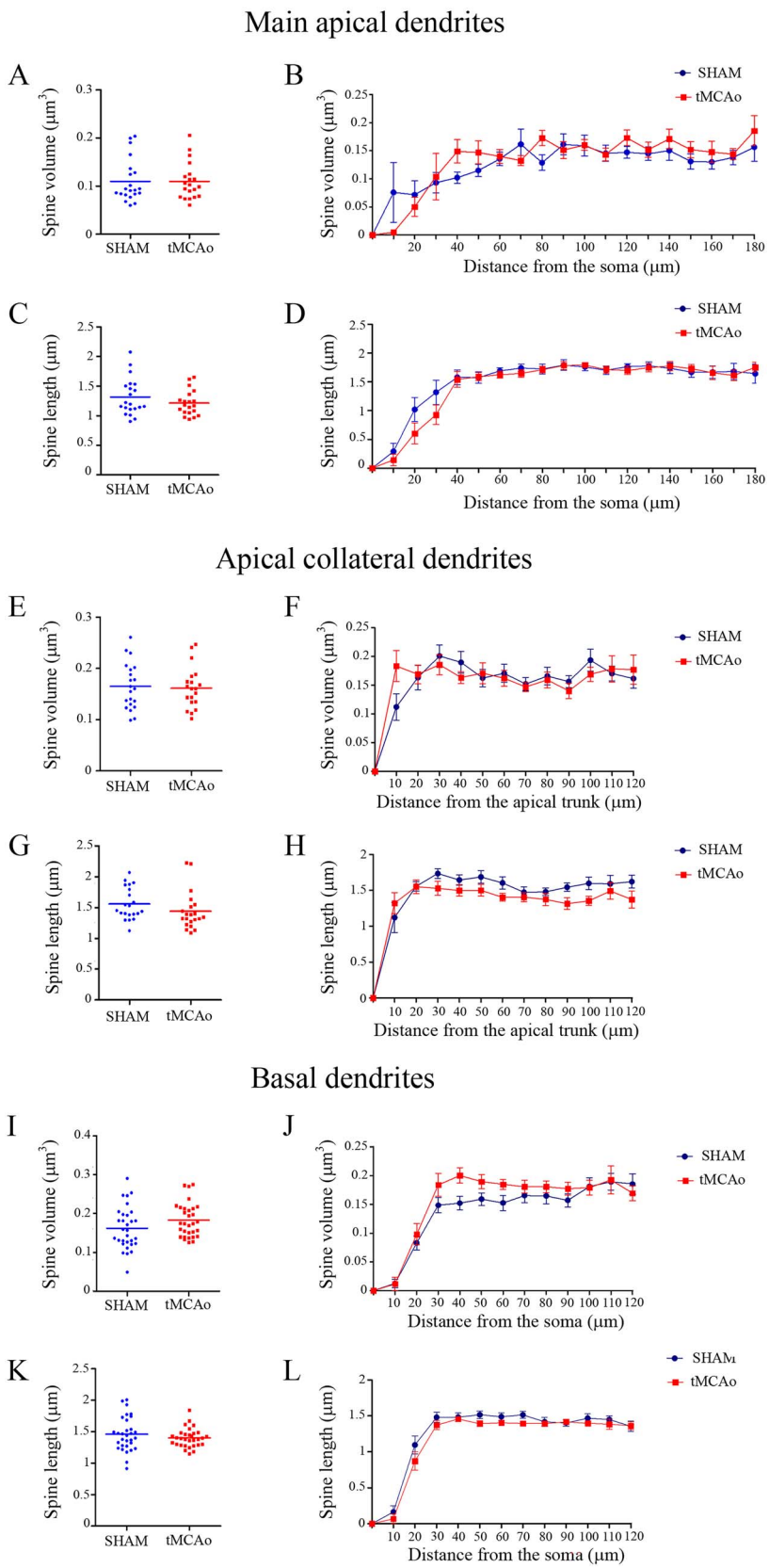

Fig. 7. Comparative morphometric analysis of dendritic spines from pyramidal neurons in the contralesional SSCx. Analysis of (A, B, E, F, I, J) spine volume and (C, D, G, H, K, L) spine length for LY-injected pyramidal neurons in sham-operated and tMCAo mice for A–D) main apical, E–H) apical collateral, and I–L) basal dendrites. Data are shown as average per dendrite (A, C, E, G, I and K; unpaired Mann–Whitney test) and as a function of the distance from the soma (B, D, F, H, J and L, Two-way ANOVA repeated measures).

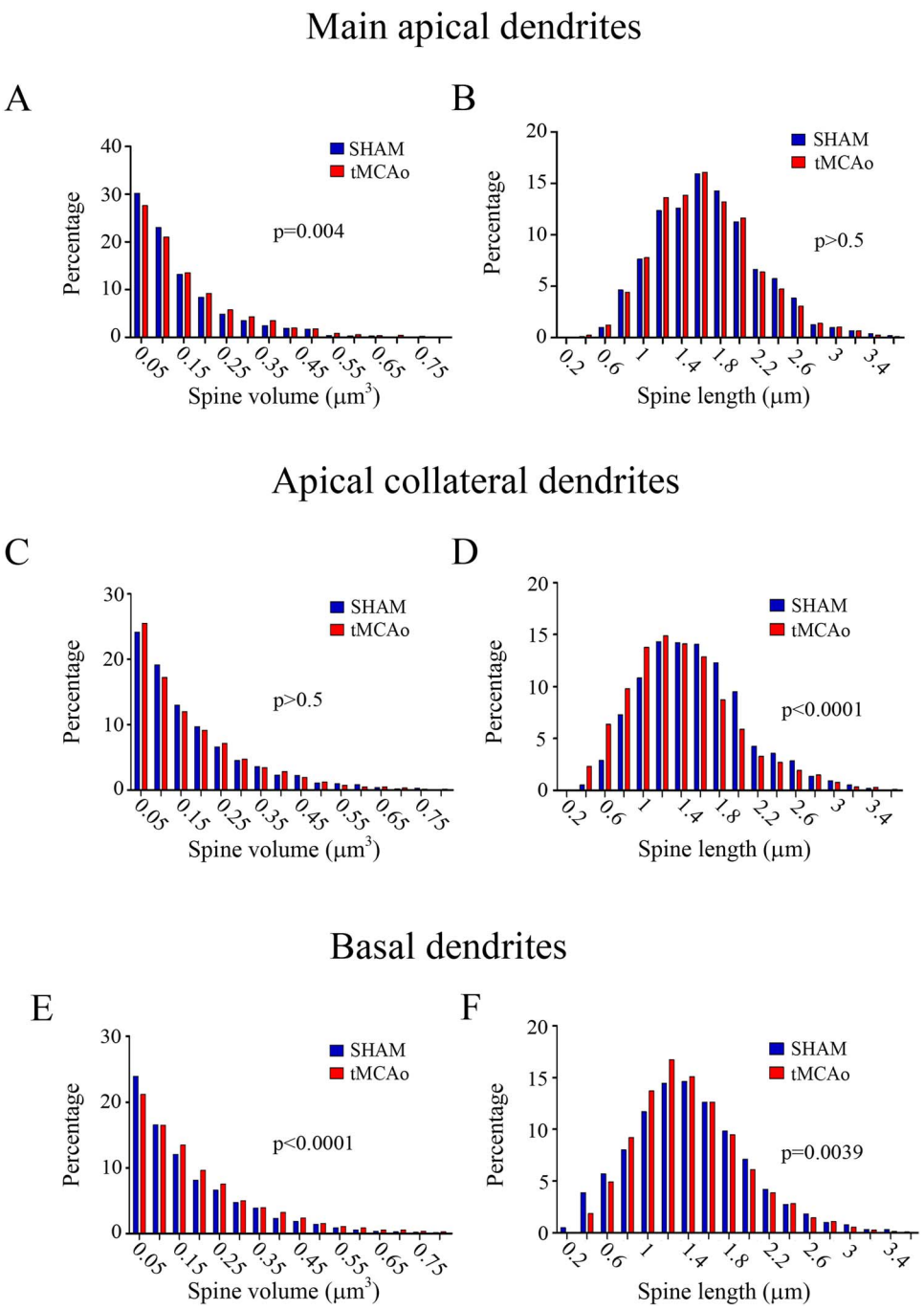

Fig. 8. Frequency distribution analysis of dendritic spine morphology. Comparative morphometric analysis of dendritic spine volume A, C, E) and spine length B, D, F) for LY-injected pyramidal neurons in sham-operated and tMCAo mice for main apical A, B), apical collateral C, D), and basal E, F) dendrites (Kolmogorov–Smirnov test).

zation and neuronal plasticity are considered the key processes involved in brain recovery after stroke (Grefkes and Fink 2020). It is well known that the adaptation of the adult brain after stroke depends on the reorganization of surviving areas adjacent to the focal lesion, which are described as highly plastic areas exposed to neuronal rewiring (Carmichael et al. 2005; Li and Carmichael 2006; Brown et al. 2007, 2010). Moreover, there are studies showing that adjacent areas adopt new roles to compensate for the loss of function in the infarcted area (Dijkhuizen et al. 2001; Ling et al. 2001; Jaillard et al. 2005). It is also known that due to the diaschisis process, remote regions connected to the infarcted area are also altered after stroke. In this regard, it has been described that the contralesional hemisphere is indeed affected, but the plastic events underlying the pathological process in the remote regions remain relatively unexplored (Duering et al. 2012; Silasi and Murphy 2014; Buetefisch 2015). This type of diaschisis is known as transcallosal diaschisis (Reggia 2004). In the interhemispheric communication, the corpus callosum represents the largest commissure in the brain. Moreover, the loss of excitatory inputs from

the damaged cerebral hemisphere to the intact contralateral cerebral cortex sent by the corpus callosum is considered as the primary mechanism responsible for transcallosal diaschisis (Ruan et al. 2017).

In the present study, we show—in a mouse model of ischemic stroke—that the pyramidal neurons in layer III of the SSCx in the contralesional hemisphere exhibit selective microanatomical alterations; we found lower neuronal complexity in the apical dendritic arbor (including a significantly lower dendritic length and dendritic volume) and spine morphological differences in main apical, apical collateral, and basal dendrites.

Alterations in the neuronal complexity and spine density of pyramidal neurons after stroke have been previously described in the peri-infarct zone (Gonzalez and Kolb 2003; Corbett et al. 2006; Ito Umeo et al. 2006; Brown et al. 2007). However, our results show—for the first time—that acute stroke selectively impairs neuronal and spine morphology in remote regions connected to the infarcted area.

It is well established that the integration of inputs within dendritic arbors is determined by factors such as the pattern of the neuronal dendritic branch. Moreover, the neuronal complexity influences the biophysical properties of the neuron, thereby regulating its functional capacity (Koch et al. 1982; London and Häusser 2005; van Elburg and van Ooyen 2010; Koleske 2013). Therefore, taking into consideration the results shown, the present study suggests a pyramidal cell dysfunction in the SSCx of the contralesional hemisphere after acute stroke in the tMCAo model. These alterations are presumably due to a loss of excitatory inputs from the damaged cerebral area to the contralateral region. It should be noted that we found a significant reduction in the neuronal complexity of the apical dendritic arbor but no differences in the basal dendritic arbor. Numerous studies have shown that the basal and apical dendritic arborizations from a single neuron collect specific synaptic inputs, with involvement in different information integrations and synaptic circuitries (DeFelipe and Fariñas 1992; Spruston 2008; Larkum 2013; Harris and Shepherd 2015; Mel et al. 2017; Aru et al. 2020; Gidon et al. 2020).

Regarding pyramidal neurons of layer III from the SSCx, different patterns of connections for the basal and apical trees have been shown. The basal dendritic tree of these neurons receives input mainly from layer IV neurons of its own cortical column, thus making connections at the local level. However, the apical dendritic trees of layer III neurons receive inputs from all the upper cortical layers, as far as layer I, which receive information from more distant areas, including the contralateral cortex (Feldmeyer 2012). Thus, our findings suggest that after an ischemic stroke, circuits involving apical and basal dendrites in the SSCx may be affected differently at the single-cell level.

Further physiological studies would be necessary to examine the potential impact of these morphological changes on the functional features of the contralateral pyramidal neurons.

We have also found that apical and basal dendrites show on average no differences in spine volume or length compared to the sham-operated animals. However, significant differences in frequency distribution of length and volume were found in the main apical, apical collateral, and basal dendrites. We do not know the functional significance of this differential distribution, but it could be the consequence of the high capacity of spines for plasticity (Yuste 2010; Ghani et al. 2017; Segal 2017), especially in the spines from the SSCx of adult mouse brain (Holtmaat et al. 2005). In this regard, using in vivo imaging, it has been demonstrated that the spines in the peri-infarct zone exhibit high plasticity that could contribute to brain recovery after injury (Brown et al. 2007).

Moreover, since spines are considered as the major postsynaptic elements of excitatory glutamatergic synapses (DeFelipe and Fariñas 1992; Harris and Kater 1994; DeFelipe 2015), we have also explored the possibility of spine dysfunction. We addressed this question by estimating the number of synaptopodin-positive puncta in the contralateral SSCx. Synaptopodin is a postsynaptic protein mainly found within the spines, specifically located in the spine apparatus—typically in large spines. The function of this protein seems to be crucial for spine plasticity, and microanatomical changes could be indicative of spine dysfunction (Deller et al. 2003; Czarnecki et al. 2005; Okubo-Suzuki et al. 2008; Vlachos et al. 2008; Jedlicka et al. 2009; Grigoryan and Segal 2016; Konietzny et al. 2019). We found no differences between tMCAo and sham-operated animals with regard to the density of synaptopodin-positive puncta. These results suggest that large spines endowed with spine apparatus are not affected in the contralesional hemisphere following medial cerebral artery occlusion, and thus, the synaptic function of this specific group of spines seems to be unaltered.

Our results show for the first time that areas that are remote from the infarct zone exhibit alterations in neuronal complexity and distribution of spines regarding their volume and length. Nevertheless, it should be noted that the method used to induce the ischemic lesion may induce remarkable differences in cortical and subcortical plasticity between studies (Gonzalez and Kolb 2003). In conclusion, the present results support the hypothesis that remote regions directly or indirectly connected to the peri-infarcted area are also affected after a stroke. However, additional experiments should be performed to further confirm the present results under other experimental conditions. For example, further tract-tracing experiments should examine whether neurons that project directly to the lesion side are more severely affected than the adjacent pyramidal neurons that do not project to the ischemic region. These experiments would help better understand the changes in brain

circuits after stroke, which would facilitate the search for more effective therapeutic approaches.

Acknowledgments

We would like to thank Carmen Álvarez and Lorena Valdés for their helpful assistance and Nick Guthrie for his excellent text editing.

Supplementary Material

Supplementary material is available at *Cerebral Cortex* online.

Funding

This work was supported by the following grants: Network of European Funding for Neuroscience Research (ERA-NET NEURON, PCI2018-092874), the Spanish Ministerio de Ciencia, Innovación y Universidades (grant IJCI-2016-27658 to P.M.S. and grant PGC2018-094307-B-I00 to J.D.), the Interdisciplinary Platform Cajal Blue Brain (CSIC, Spain), the Centro de Investigación Biomédica en Red sobre Enfermedades Neurodegenerativas (CIBERNED, CB06/05/0066, Spain) and the Deutsche Forschungsgemeinschaft (DFG, German Research Foundation) under Germany's Excellence Strategy within the framework of the Munich Cluster for Systems Neurology (EXC 2145 SyNergy – ID 390857198) to NP.

Conflict of interest statement. The authors declare that they have no competing interest.

References

Aru J, Suzuki M, Larkum ME. Cellular mechanisms of conscious processing. *Trends Cogn Sci*. 2020:24:814–825.

Ballesteros-Yáñez I, Benavides-Piccione R, Bourgeois J-P, Changeux J-P, DeFelipe J. Alterations of cortical pyramidal neurons in mice lacking high-affinity nicotinic receptors. *Proc Natl Acad Sci U S A*. 2010:107:11567–11572.

Barbas H. General cortical and special prefrontal connections: principles from structure to function. *Annu Rev Neurosci*. 2015:38: 269–289.

Benavides-Piccione R, Hamzei-Sichani F, Ballesteros-Yáñez I, DeFelipe J, Yuste R. Dendritic size of pyramidal neurons differs among mouse cortical regions. *Cereb Cortex*. 2006:16:990–1001.

Benavides-Piccione R, Fernaud-Espinosa I, Robles V, Yuste R, DeFelipe J. Age-based comparison of human dendritic spine structure using complete three-dimensional reconstructions. *Cereb Cortex*. 2013:23:1798–1810.

Benavides-Piccione R, Regalado-Reyes M, Fernaud-Espinosa I, Kastanauskaite A, Tapia-González S, León-Espinosa G, Rojo C, Insausti R, Segev I, DeFelipe J. Differential structure of hippocampal CA1 pyramidal neurons in the human and mouse. *Cereb Cortex*. 2020:30(2):730–752.

Bourne J, Harris KM. Do thin spines learn to be mushroom spines that remember? *Curr Opin Neurobiol*. 2007:17:381–386.

Brecht M. The body model theory of somatosensory cortex. *Neuron*. 2017:94:985–992.

Brown CE, Li P, Boyd JD, Delaney KR, Murphy TH. Extensive turnover of dendritic spines and vascular remodeling in cortical tissues recovering from stroke. *J Neurosci*. 2007:27:4101–4109.

Brown CE, Boyd JD, Murphy TH. Longitudinal in vivo imaging reveals balanced and branch-specific remodeling of mature cortical pyramidal dendritic arbors after stroke. *J Cereb Blood Flow Metab*. 2010:30:783–791.

Buetefisch CM. Role of the contralesional hemisphere in post-stroke recovery of upper extremity motor function. *Front Neurol*. 2015:6:214.

Butz M, Steenbuck ID, van Ooyen A. Homeostatic structural plasticity can account for topology changes following deafferentation and focal stroke. *Front Neuroanat*. 2014:8:115.

Carmichael ST, Archibeque I, Luke L, Nolan T, Momiy J, Li S. Growth-associated gene expression after stroke: evidence for a growth-promoting region in peri-infarct cortex. *Exp Neurol*. 2005:193: 291–311.

Chovsepian A, Empl L, Correa D, Bareyre FM. Heterotopic transcallosal projections are present throughout the mouse cortex. *Front Cell Neurosci*. 2017:11:36.

Corbett D, Giles T, Evans S, McLean J, Biernaskie J. Dynamic changes in CA1 dendritic spines associated with ischemic tolerance. *Exp Neurol*. 2006:202:133–138.

Czarnecki K, Haas CA, Orth CB, Deller T, Frotscher M. Postnatal development of synaptopodin expression in the rodent hippocampus. *J Comp Neurol*. 2005:490:133–144.

D'Souza RD, Burkhalter A. A laminar organization for selective cortico-cortical communication. *Front Neuroanat*. 2017:11:71.

DeFelipe J. The evolution of the brain, the human nature of cortical circuits, and intellectual creativity. *Front Neuroanat*. 2011:5: 29.

DeFelipe J. The dendritic spine story: an intriguing process of discovery. *Front Neuroanat*. 2015:9:14.

DeFelipe J, Fariñas I. The pyramidal neuron of the cerebral cortex: morphological and chemical characteristics of the synaptic inputs. *Prog Neurobiol*. 1992:39:563–607.

Deller T, Korte M, Chabanis S, Drakew A, Schwegler H, Stefani GG, Zuniga A, Schwarz K, Bonhoeffer T, Zeller R, et al. Synaptopodin-deficient mice lack a spine apparatus and show deficits in synaptic plasticity. *PNAS*. 2003:100:10494–10499.

Dijkhuizen RM, Ren J, Mandeville JB, Wu O, Ozdag FM, Moskowitz MA, Rosen BR, Finklestein SP. Functional magnetic resonance imaging of reorganization in rat brain after stroke. *PNAS*. 2001:98: 12766–12771.

Donnan GA, Fisher M, Macleod M, Davis SM. Stroke. *Lancet*. 2008:371: 1612–1623.

Duering M, Righart R, Csanadi E, Jouvent E, Hervé D, Chabriat H, Dichgans M. Incident subcortical infarcts induce focal thinning in connected cortical regions. *Neurology*. 2012:79:2025–2028.

Feigin VL, Bo N, Mensah GA. Global burden of stroke. *Circ Res*. 2017:120:439–448.

Feldmeyer D. Excitatory neuronal connectivity in the barrel cortex. *Front Neuroanat*. 2012:6:24.

Fenlon LR, Suárez R, Richards LJ. The anatomy, organisation and development of contralateral callosal projections of the mouse somatosensory cortex. *Brain Neurosci Adv*. 2017:1:2398212817694888.

Freund TF, Buzsáki G, Leon A, Baimbridge KG, Somogyi P. Relationship of neuronal vulnerability and calcium binding protein immunoreactivity in ischemia. *Exp Brain Res*. 1990:83:55–66.

Ghani MU, Mesadi F, Kanık SD, Argunşah AÖ, Hobbiss AF, Israely I, Ünay D, Taşdizen T, Çetin M. Dendritic spine classification using shape and appearance features based on two-photon microscopy. *J Neurosci Methods*. 2017:279:13–21.

Gidon A, Zolnik TA, Fidzinski P, Bolduan F, Papoutsi A, Poirazi P, Holtkamp M, Vida I, Larkum ME. Dendritic action potentials

and computation in human layer 2/3 cortical neurons. *Science*. 2020:367:83–87.

Gonzalez CLR, Kolb B. A comparison of different models of stroke on behaviour and brain morphology. *Eur J Neurosci*. 2003:18: 1950–1962.

Grefkes C, Fink GR. Recovery from stroke: current concepts and future perspectives. *Neurol Res Pract*. 2020:2:17.

Grigoryan G, Segal M. Ryanodine-mediated conversion of STP to LTP is lacking in synaptopodin-deficient mice. *Brain Struct Funct*. 2016:221:2393–2397.

Harris KM, Kater SB. Dendritic spines: cellular specializations imparting both stability and flexibility to synaptic function. *Annu Rev Neurosci*. 1994:17:341–371.

Harris KD, Shepherd GMG. The neocortical circuit: themes and variations. *Nat Neurosci*. 2015:18:170–181.

Häusser M, Spruston N, Stuart GJ. Diversity and dynamics of dendritic Signaling. *Science*. 2000:290:739–744.

Holtmaat AJGD, Trachtenberg JT, Wilbrecht L, Shepherd GM, Zhang X, Knott GW, Svoboda K. Transient and persistent dendritic spines in the neocortex in vivo. *Neuron*. 2005:45:279–291.

Jaillard A, Martin CD, Garambois K, Lebas JF, Hommel M. Vicarious function within the human primary motor cortex?: a longitudinal fMRI stroke study. *Brain*. 2005:128:1122–1138.

Jeannette H, van Putten MJAM. Ischemic cerebral damage. *Stroke*. 2012:43:607–615.

Jedlicka P, Schwarzacher SW, Winkels R, Kienzler F, Frotscher M, Bramham CR, Schultz C, Orth CB, Deller T. Impairment of in vivo theta-burst long-term potentiation and network excitability in the dentate gyrus of synaptopodin-deficient mice lacking the spine apparatus and the cisternal organelle. *Hippocampus*. 2009:19:130–140.

Jia H, Rochefort NL, Chen X, Konnerth A. Dendritic organization of sensory input to cortical neurons in vivo. *Nature*. 2010:464: 1307–1312.

Kandel ER, Dudai Y, Mayford MR. The molecular and systems biology of memory. *Cell*. 2014:157:163–186.

Kilkenny C, Browne WJ, Cuthill IC, Emerson M, Altman DG. Improving bioscience research reporting: the ARRIVE guidelines for reporting animal research. *PLoS Biol*. 2010:8(6):e1000412.

Koch C, Poggio T, Torre V, Boycott BB. Retinal ganglion cells: a functional interpretation of dendritic morphology. *Philos Trans R Soc Lond B Biol Sci*. 1982:298:227–263.

Koleske AJ. Molecular mechanisms of dendrite stability. *Nat Rev Neurosci*. 2013:14:536–550.

Konietzny A, González-Gallego J, Bär J, Perez-Alvarez A, Drakew A, Demmers JAA, Dekkers DHW, Hammer JA, Frotscher M, Oertner TG, et al. Myosin V regulates synaptopodin clustering and localization in the dendrites of hippocampal neurons. *J Cell Sci*. 2019: 132(16):jcs230177.

Kropf E, Syan SK, Minuzzi L, Frey BN. From anatomy to function: the role of the somatosensory cortex in emotional regulation. *Braz J Psychiatry*. 2018:41:261–269.

Larkum M. A cellular mechanism for cortical associations: an organizing principle for the cerebral cortex. *Trends Neurosci*. 2013:36: 141–151.

Leguey I, Benavides-Piccione R, Rojo C, Larrañaga P, Bielza C, DeFelipe J. Patterns of dendritic basal field orientation of pyramidal neurons in the rat somatosensory cortex. *eNeuro*. 2018:5(6):ENEURO.0142–18.2018.

Li S, Carmichael ST. Growth-associated gene and protein expression in the region of axonal sprouting in the aged brain after stroke. *Neurobiol Dis*. 2006:23:362–373.

Lin C-S, Polsky K, Nadler JV, Crain BJ. Selective neocortical and thalamic cell death in the gerbil after transient ischemia. *Neuroscience*. 1990:35:289–299.

Lin Y-H, Liang H-Y, Xu K, Ni H-Y, Dong J, Xiao H, Chang L, Wu H-Y, Li F, Zhu D-Y, et al. Dissociation of nNOS from PSD-95 promotes functional recovery after cerebral ischaemia in mice through reducing excessive tonic GABA release from reactive astrocytes. *J Pathol*. 2018:244:176–188.

Ling W, Erinjeri JP, Rovainen CM, Woolsey TA. Collateral growth and angiogenesis around cortical stroke. *Stroke*. 2001:32:2179–2184.

London M, Häusser M. Dendritic computation. *Annu Rev Neurosci*. 2005:28:503–532.

Lourbopoulos A, Mamrak U, Roth S, Balbi M, Shrouder J, Liesz A, Hellal F, Plesnila N. Inadequate food and water intake determine mortality following stroke in mice. *J Cereb Blood Flow Metab*. 2017:37:2084–2097.

Mel BW, Schiller J, Poirazi P. Synaptic plasticity in dendrites: complications and coping strategies. *Curr Opin Neurobiol*. 2017:43: 177–186.

Okubo-Suzuki R, Okada D, Sekiguchi M, Inokuchi K. Synaptopodin maintains the neural activity-dependent enlargement of dendritic spines in hippocampal neurons. *Mol Cell Neurosci*. 2008:38: 266–276.

Reggia JA. Neurocomputational models of the remote effects of focal brain damage. *Med Eng Phys*. 2004:26:711–722.

Rockland KS. What do we know about laminar connectivity? *NeuroImage*. 2019:197:772–784.

Ruan L, Wang Y, Chen S, Zhao T, Huang Q, Hu Z, Xia N, Liu J, Chen W, Zhang Y, et al. Metabolite changes in the ipsilateral and contralateral cerebral hemispheres in rats with middle cerebral artery occlusion. *Neural Regen Res*. 2017:12:931–937.

Segal M. Dendritic spines: morphological building blocks of memory. *Neurobiol Learn Mem*. 2017:2017(138):3–9.

Silasi G, Murphy TH. Stroke and the connectome: how connectivity guides therapeutic intervention. *Neuron*. 2014:83: 1354–1368.

Spruston N. Pyramidal neurons: dendritic structure and synaptic integration. *Nat Rev Neurosci*. 2008:9:206–221.

Stuart GJ, Spruston N. Dendritic integration: 60 years of progress. *Nat Neurosci*. 2015:18:1713–1721.

Takamatsu Y, Tamakoshi K, Waseda Y, Ishida K. Running exercise enhances motor functional recovery with inhibition of dendritic regression in the motor cortex after collagenase-induced intracerebral hemorrhage in rats. *Behav Brain Res*. 2016:300: 56–64.

Tang LT, Diaz-Balzac CA, Rahman M, Ramirez-Suarez NJ, Salzberg Y, Lázaro-Peña MI, Bülow HE. TIAM-1/GEF can shape somatosensory dendrites independently of its GEF activity by regulating F-actin localization. *Elife*. 2019:8:e38949.

Umeo I, Toshihiko K, Jun N, Emiko K, Kiyomitsu O. Temporal profiles of axon terminals, synapses and spines in the ischemic penumbra of the cerebral cortex. *Stroke*. 2006:37:2134–2139.

van Elburg RAJ, van Ooyen A. Impact of dendritic size and dendritic topology on burst firing in pyramidal cells. *PLoS Comput Biol*. 2010:6:e1000781.

Vlachos A, Maggio N, Segal M. Lack of correlation between synaptopodin expression and the ability to induce LTP in the rat dorsal and ventral hippocampus. *Hippocampus*. 2008:18:1–4.

Wen Q, Stepanyants A, Elston GN, Grosberg AY, Chklovskii DB. Maximization of the connectivity repertoire as a statistical principle governing the shapes of dendritic arbors. *PNAS*. 2009:106: 12536–12541.

Xie Q, Cheng J, Pan G, Wu S, Hu Q, Jiang H, Wang Y, Xiong J, Pang Q, Chen X. Treadmill exercise ameliorates focal cerebral ischemia/reperfusion-induced neurological deficit by promoting dendritic modification and synaptic plasticity via upregulating caveolin-1/VEGF signaling pathways. *Exp Neurol*. 2019:313:60–78.

Yuste R. *Dendritic spines*. Cambridge, MA: MIT Press; 2010

Zhu L, Wang L, Ju F, Khan A, Cheng X, Zhang S. Reversible recovery of neuronal structures depends on the degree of neuronal damage after global cerebral ischemia in mice. *Exp Neurol*. 2017:289: 1–8.